

Desorption of CO and O₂ interstellar ice analogs

K. Acharyya^{1,2}, G.W. Fuchs¹, H.J. Fraser³, E.F. van Dishoeck¹, and H. Linnartz¹

¹ Raymond and Beverly Sackler Laboratory for Astrophysics, Leiden Observatory, Leiden University, Postbus 9513, NL 2300 RA Leiden, The Netherlands
e-mail: acharyya@strw.leidenuniv.nl

² Centre For Space Physics, 43 Chalantika, Garia, Kolkata, 720084, India

³ Department of Physics SUPA (Scottish Universities Physics Alliance), University of Strathclyde, 107 Rottenrow East, Glasgow G4 ONG, Scotland

07/08/2006

ABSTRACT

Context.

Aims. Solid O₂ has been proposed as a possible reservoir for oxygen in dense clouds through freeze-out processes. The aim of this work is to characterize quantitatively the physical processes that are involved in the desorption kinetics of CO-O₂ ices by interpreting laboratory temperature programmed desorption (TPD) data. This information is used to simulate the behavior of CO-O₂ ices under astrophysical conditions.

Methods. The TPD spectra have been recorded under ultra high vacuum conditions for pure, layered and mixed morphologies for different thicknesses, temperatures and mixing ratios. An empirical kinetic model is used to interpret the results and to provide input parameters for astrophysical models.

Results. Binding energies are determined for different ice morphologies. Independent of the ice morphology, the desorption of O₂ is found to follow 0th-order kinetics. Binding energies and temperature-dependent sticking probabilities for CO-CO, O₂-O₂ and CO-O₂ are determined. O₂ is slightly less volatile than CO, with binding energies of 912±15 versus 858±15 K for pure ices. In mixed and layered ices, CO does not co-desorb with O₂ but its binding energies are slightly increased compared with pure ice whereas those for O₂ are slightly decreased. Lower limits to the sticking probabilities of CO and O₂ are 0.9 and 0.85, respectively, at temperatures below 20 K. The balance between accretion and desorption is studied for O₂ and CO in astrophysically relevant scenarios. Only minor differences are found between the two species, i.e., both desorb between 16 and 18 K in typical environments around young stars. Thus, clouds with significant abundances of gaseous CO are unlikely to have large amounts of solid O₂.

Conclusions.

Key words. dust, extinction - ISM: molecules - ices – methods: laboratory - molecular data - molecular processes

1. Introduction

Gas-grain interactions play a key role in the chemical evolution of star-forming regions. During the first stages of star formation virtually all species accrete onto grains in dense cold cores. Later on in the star formation sequence — when so-called hot cores are formed — grains are warmed to temperatures where molecules can desorb again. In order to characterize this astrophysical process quantitatively it is necessary to understand the underlying molecular physics by studying interstellar ice analogs under laboratory controlled conditions. A series of recent papers shows that even for simple molecules such a quantification is far from trivial (e.g. Fraser et al. 2001, Collings et al. 2003, 2004, Öberg et al. 2005, Bisschop et al. 2006). In the present work results for CO and O₂ ices are discussed that extend recent work comparing CO-N₂ and CO-O₂ ice features (Fuchs et al. 2006) to an empirical kinetic model characterizing the desorption behavior.

The reason for focusing on ices containing O₂ is that a substantial amount of interstellar oxygen may well freeze out onto grains in the form of molecular oxygen. Attempts to determine gaseous O₂-abundances from recent SWAS and ODIN campaigns put upper limits on the O₂ abun-

dance in cold dark clouds in the range of 3×10^{-6} - 1×10^{-7} (Goldsmith et al. 2000, Pagani et al. 2003, Liseau et al. 2005). This low abundance, along with the low abundance of gaseous H₂O, raises serious questions about the total oxygen budget when compared with the well observed atomic oxygen abundance of 3×10^{-4} in diffuse clouds (Meyer et al. 1998, Ehrenfreund & van Dishoeck 1998). One possible explanation for the ‘missing’ oxygen is that it is frozen out onto grains in the coldest regions. The fundamental vibration of solid O₂ around 1550 cm^{-1} ($6.45 \mu\text{m}$) becomes observable through perturbations of the symmetry of O₂ in a matrix or ice containing other molecules (Ehrenfreund et al. 1992). This band has been sought towards the proto-stellar sources RCrA IRS2 and NGC 7538 IRS9 (Vandenbussche et al. 1999), but not detected. Upper limits between 50% and 100% of solid O₂ relative to solid CO have been reported from analysis of the CO profile, since solid CO, in contrast with solid O₂, has been observed through its vibrational band at $4.67 \mu\text{m}$ (2140 cm^{-1}) (e.g. Chiar et al. 1998, Pontoppidan et al. 2003). Here the amount of frozen O₂ can be estimated by observing its influence on the shape of the CO absorption band. Transmission spectra recorded for mixed CO-O₂ ices show indeed significant changes compared to pure CO ices (Ehrenfreund et

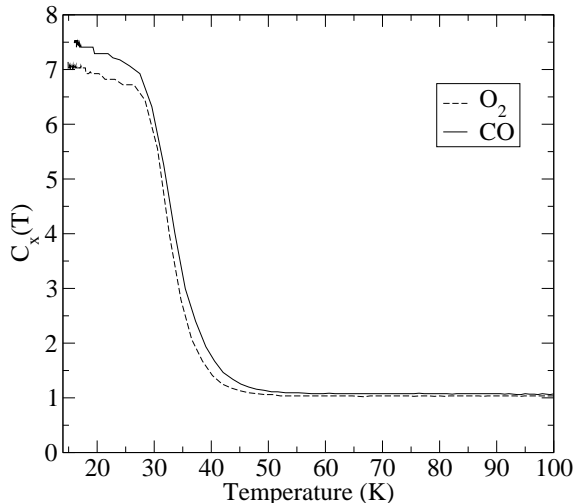


Fig. 1. The cryo-pumping factor ($C_x(T) = p_{rt}/p_t$) as a function of temperature for CO (solid) and O₂ (dashed).

al. 1997, Elsila et al. 1997). However, such changes can also be caused by grain size and shape effects (Dartois 2006). The best limits on solid O₂ therefore come from analysis of the weak solid ¹³CO band which is not affected by grain shape effects. This band leads to upper limits of 100% on the amount of O₂ that can be mixed with CO (Boogert et al. 2003, Pontoppidan et al. 2003).

In this study, laboratory results for CO-O₂ ices are presented, both in pure, layered and mixed ice morphologies for varying ice thicknesses and for different relative abundances (Section 2). The focus is on temperature programmed desorption (TPD) data that are recorded to study the desorption process and to visualize changes in ice morphology during heating (Section 3). An empirical kinetic model is used to interpret the TPD data (Section 4). The aim of this work is to derive accurate molecular parameters (CO-CO, CO-O₂ and O₂-O₂ binding energies, classification of desorption kinetics, and temperature dependent sticking coefficients) to allow reliable predictions of typical behavior under astrophysical conditions (Section 5).

2. Experiment

The experimental setup consists of an ultra-high vacuum setup (background pressure $< 5 \times 10^{-11}$ mbar) in which interstellar ice analogs are grown with mono-layer precision on a 2.5×2.5 cm² sample surface made out of a 0.1 μ m thick polycrystalline gold film. Physical-chemical interactions can be studied using TPD and/or reflection absorption infrared spectroscopy (RAIRS). Details of the setup are available from van Broekhuizen (2005) and Fuchs et al. (2006) and here only relevant details are given. We assume that for a sticking coefficient of 1, molecules hitting the cold surface (14 K) build up one monolayer (ML) at a steady gas exposure of $1.33 \cdot 10^{-6}$ mbar s⁻¹ (10^{-6} Torr s⁻¹). This is by definition one Langmuir [L] and corresponds to roughly 10^{15} particles cm⁻² in a non-porous condensed solid. In the present experiment amorphous ice is grown using a 0.01 L s⁻¹ growth velocity resulting in a well specified layer thick-

Table 1. Overview of all ice morphologies used in the CO-O₂ experiments. The thickness is given in Langmuir [L].

| | ¹³ CO | ¹⁸ O ₂ | Total | ¹² CO | ¹⁶ O ₂ | Total |
|---|------------------|------------------------------|-------|------------------|------------------------------|-------|
| CO pure | 20 | - | 20 | 20 | - | 20 |
| | 40 | - | 40 | 40 | - | 40 |
| | 60 | - | 60 | - | - | - |
| | 80 | - | 80 | 80 | - | 80 |
| O ₂ pure | - | 20 | 20 | - | 20 | 20 |
| | - | 40 | 40 | - | 40 | 40 |
| | - | 60 | 60 | - | - | - |
| | - | 80 | 80 | - | 80 | 80 |
| CO:O ₂ mixed | 20 | 20 | 40 | - | - | - |
| | 30 | 30 | 60 | - | - | - |
| | 40 | 40 | 80 | 40 | 40 | 80 |
| | 60 | 60 | 120 | - | - | - |
| | 80 | 80 | 160 | - | - | - |
| O ₂ /CO ^a layered | 20 | 20 | 40 | 20 | 20 | 40 |
| | 30 | 30 | 60 | - | - | 80 |
| | 40 | 40 | 80 | 40 | 40 | 80 |
| | 60 | 60 | 120 | - | - | - |
| | 80 | 80 | 160 | 80 | 80 | - |
| | 40 | 5 | 45 | - | - | - |
| | 40 | 10 | 50 | 40 | 10 | 50 |
| | 40 | 20 | 60 | 40 | 20 | 60 |
| | 40 | 30 | 70 | - | - | - |
| | 40 | 40 | 80 | - | - | - |
| CO/O ₂ ^a layered | 20 | 20 | 40 | - | - | 40 |
| | 40 | 40 | 80 | 40 | 40 | 80 |
| | 80 | 80 | 160 | - | - | - |

^a See text for explanation of the used notation.

ness as long as the growth is linear with the exposure time. Typical layer thicknesses are generated in the range between 20 and 80 L as astrophysical observations of young stellar objects in nearby low-mass star-forming clouds indicate that CO ices exist at thicknesses around 40 monolayers (Pontoppidan et al. 2003). In addition, astrochemical models suggest that O₂ may freeze out onto a pre-existing CO layer and consequently both pure, mixed and layered ices are studied here (Hasegawa et al. 1992, d’Hendecourt et al. 1985, Bergin et al. 2000). Studies of O₂ in an H₂O-rich environment have been performed by Collings et al. (2004).

Two sets of ices have been investigated, ¹³CO-¹⁸O₂ and ¹²CO-¹⁶O₂, both using isotopes of at least 99% purity. Most experiments were performed using ¹³CO-¹⁸O₂ to distinguish between possible impurities in the vacuum system. An overview of the used ice samples is given in Table 1. Throughout this paper, the notation x/y and x:y denote layered (x on top of y) and mixed ice morphologies, respectively. The notation 1/1 indicates layered ices of equal thickness, 1:1 refers to equally mixed ices and x/40 L stands for ices where the thickness of the top layer is varied by x L and the bottom layer is kept constant at 40 L.

Once an ice is grown the desorption behavior is examined by a controlled linear temperature rise from 12 to 80 K. The heating rate in all experiments is 0.1 K min⁻¹, unless stated differently. The CO and O₂ molecules that are released are monitored by a quadrupole mass spectrometer (QMS). For a constant pumping speed the QMS signal strengths are proportional to the amount of desorbed species. Since the deposition surface, together with other cold surface areas like the radiation shield, can be regarded as a cryogenic pump a temperature dependent cryo-pump

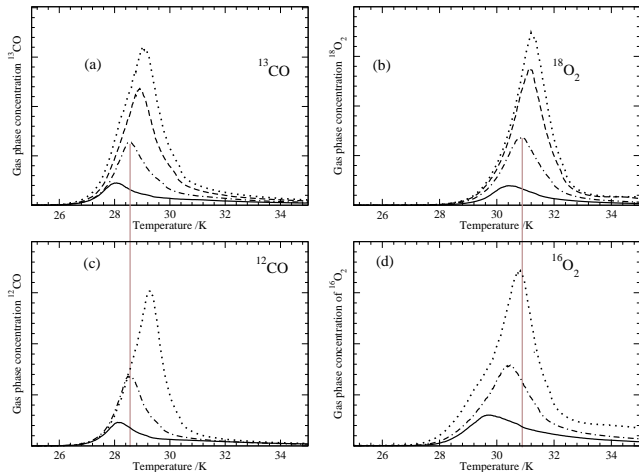


Fig. 2. TPD spectra of pure ices. (a) ^{13}CO and (b) $^{18}\text{O}_2$ - for exposures of 20 L (solid), 40 L (dot-dashed), 60 L (dashed) and 80 L (dotted) - and (c) ^{12}CO and (d) $^{16}\text{O}_2$ - for exposures of 20 L (solid), 40 L (dot-dashed) and 80 L (dotted). The grey vertical lines indicate the peak temperatures at 40 L.

factor has to be introduced as the pressure in the chamber decreases when the temperature drops below 50 K. This effect is measured by opening the leakage valve up to a certain pressure (p_{rt}) at room temperature after which the system is cooled down to 14 K and the corresponding pressure (p_t) is determined. In Fig. 1 the ratio $C_x(T) = p_{rt}/p_t$ is shown as a function of temperature for both CO and O₂ revealing that at 14 K the cryo-pumping factor increases by a factor of about 7 with respect to the pumping speed, s_{tp} , of the turbo pump alone. This effect is important and will be explicitly taken into account in the kinetic model.

Reflection-Absorption Infrared (RAIR) spectra have been taken simultaneously with the TPD data but are not included here. Spectra for selected CO-O₂ experiments were presented and discussed in Fuchs et al. (2006); they provide additional information on the processes occurring in the ice during heating.

3. Experimental results

TPD spectra of pure and mixed/layered CO-O₂ ices are shown in Figs. 2 and 3, respectively.

Pure ices. In the case of pure ^{13}CO ice (Fig. 2a) and pure ^{12}CO ice (Fig. 2c) the desorption starts around 26.5 K and peaks between 28 and 29 K. All leading edges clearly coincide and peak temperatures shift towards higher temperatures for higher thicknesses. This behavior is typical for a 0th-order desorption process (see §4.1) and corresponds to a desorption rate that is independent of the ice thickness and that remains constant until no molecules are left on the surface (see also Collings et al. 2003, Bisschop et al. 2006). The binding energies for both isotopes are similar and consequently nearly the same peak temperature is found. For pure $^{18}\text{O}_2$ ice (Fig. 2b) and pure $^{16}\text{O}_2$ ice (Fig. 2d) a similar behavior is found as for CO: all desorption curves have the same leading edges and the peak temperature slightly shifts for increasing thicknesses (from 29.5 to 31.3 K). The des-

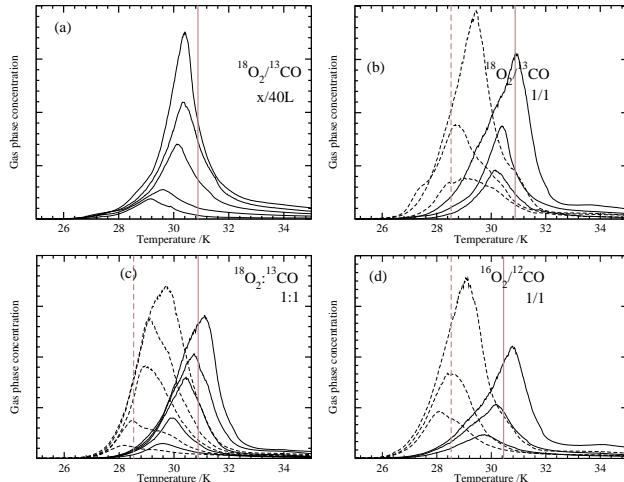


Fig. 3. TPD spectra for mixed/layered ices. (a) O₂ trace of (5, 10, 20, 30 and 40 L) $^{18}\text{O}_2/40\text{ L }^{13}\text{CO}$ - differential layer, (b) (20, 40 and 80 L) $^{18}\text{O}_2$ (solid line) and ^{13}CO (dashed line) for 1/1 O₂/CO system. (The shoulder observed in the 40 L measurement is an experimental artifact absent in other experiments). (c) (10, 20, 40, 60, 80 L) $^{18}\text{O}_2$ (solid line) and ^{13}CO (dashed line) for 1:1 mixed ices, (d) (20, 40 and 80 L) $^{16}\text{O}_2$ (solid line) and ^{12}CO (dashed line) for the 1/1 O₂/CO system. The grey vertical lines indicate the peak temperatures for pure O₂ (solid) and pure CO (dashed) for 40 L.

orption peak of O₂ is clearly shifted to higher temperatures by ~ 2 K compared with CO. A small shift of peak temperatures of less than 0.5 K is observed when comparing $^{18}\text{O}_2$ and $^{16}\text{O}_2$.

Layered ices. In Fig. 3a TPD spectra are shown for different layers of $^{18}\text{O}_2$ on top of 40 L ^{13}CO and in Fig. 3b (3d) for $^{18}\text{O}_2$ ($^{16}\text{O}_2$) on top of ^{13}CO (^{12}CO) for different 1/1 configurations (i.e. 20 L $^{18}\text{O}_2/20\text{ L }^{13}\text{CO}$, 40 L $^{16}\text{O}_2/40\text{ L }^{12}\text{CO}$, etc.). In all cases the O₂ desorption behaves as a 0th-order process and is very similar to that observed for pure O₂ ice. This can be expected as O₂ is less volatile than CO, i.e., at the desorbing temperatures of O₂ there is little CO left to influence the O₂ desorption process. The only noticeable difference compared to pure ices is that the peak temperature shifts to a lower value for O₂ and to a higher temperature for CO by about 0.5 K. This indicates that in the layered ice systems the binding energies change; for CO the binding energy increases whereas for O₂ it decreases. With exception of the 20 L ^{13}CO spectrum, all layered CO traces reveal a 0th-order process as can be seen in Fig. 3b and Fig. 3d for the ^{12}CO . Potentially, the presence of O₂ on top of the CO ice can change the desorption process for CO but RAIR spectra of layered ices do not change much with respect to pure ices. The lack of co-desorption of CO with the O₂ suggests that the molecular interaction between these species is weak.

Mixed ices. In Fig. 3c the TPD spectra are shown for different layer thicknesses of 1:1 $^{18}\text{O}_2:^{13}\text{CO}$ mixed ices. The O₂ desorption follows again a 0th-order process, but the band as a whole is slightly broadened by 10-15% compared to pure O₂. In the ^{13}CO spectra a shoulder around 29.6 K

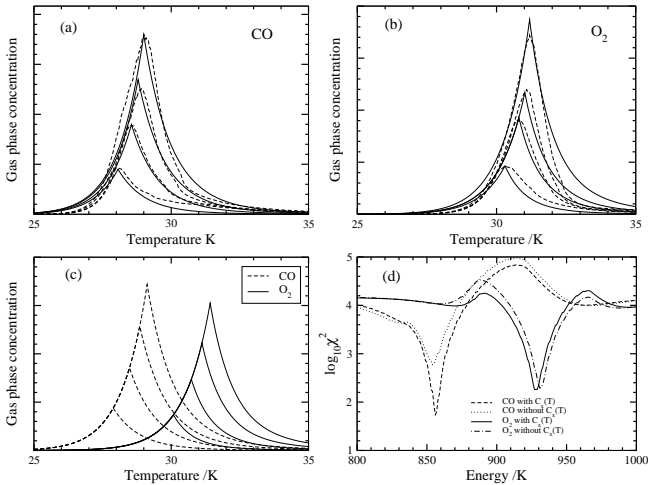


Fig. 4. Model TPD spectra of pure ice (solid lines) compared with laboratory data (dashed lines) for 20, 40, 60 and 80 L ices. (a) ¹³CO, (b) ¹⁸O₂, (c) Model ¹³CO (dashed) and ¹⁸O₂ (solid) using recommended energy values and (d) variation of χ^2 with energy for an exposure of 40 L, illustrating the well-determined minima. The effect of fits with and without using the cryo-pumping function $C_x(T)$ are shown.

appears, i.e. at the O₂ desorption temperature, which suggests that a fraction of the CO desorbs from C'O-CO binding sites like in pure ices whereas the rest desorbs from a mixed environment, e.g. CO-O₂ binding sites. The main isotopes (not shown in the figure) exhibit a similar behavior. Compared with previous experiments performed on CO-N₂ ices (Öberg et al. 2005, Bisschop et al. 2006) these results have been interpreted as follows (Fuchs et al. 2006): neither N₂ nor O₂ possess an electric dipole moment so they interact with CO mainly via quadrupole interactions. However, solid O₂ has a 4 to 6 times weaker quadrupole moment compared to N₂ and CO. Furthermore, N₂ and CO possess the same α -crystalline structure below 30 K, but α -phase O₂ has a different crystalline structure and also undergoes a phase change to the β -form at 23.5 K. The combination of these two effects can lead to the absence of mixing and co-desorption in the CO-O₂ system compared with CO-N₂, as observed in our experiments.

4. Empirical kinetic model of CO-O₂ desorption

The experimental TPD results are interpreted in terms of an empirical kinetic model, describing the desorption kinetics and providing values for fundamental molecular properties to be used in astrochemical models.

4.1. The model

The kinetic desorption process for a species X can be expressed by the well known Polanyi-Wigner type equations of the form,

$$R_{des} = \frac{dN_g(X)}{dt} = \nu_i [N_s(X)]^i \exp\left[-\frac{E_d(X)}{T}\right] \quad (1)$$

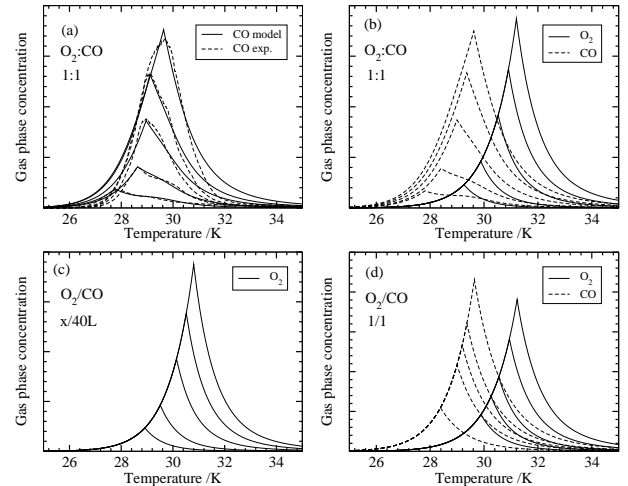


Fig. 5. Model TPD spectra of layered and mixed ices; (a) Experimental (dashed) and model (solid) results of ¹³CO in mixed ice; (b) Best fitting ¹³CO and ¹⁸O₂ model results for mixed ices; (c) Best fitting ¹⁸O₂ model results for $x/40$ L ¹⁸O₂ / ¹³CO and (d) best fitting model results for ¹³CO and ¹⁸O₂ in 1/1 layered ices.

with R_{des} the desorption rate (molecules $\text{cm}^{-2}\text{s}^{-1}$), $N_g(X)$ the number density (cm^{-2}) of molecules desorbing from the substrate, ν_i a pre-exponential factor (molecules ^{$1-i$} $\text{cm}^{2(i-1)}\text{s}^{-1}$) for desorption order i , $N_s(X)$ the number density (cm^{-2}) of molecules on the surface at a given time t , $E_d(X)$ the binding energy (in K) and T the surface temperature (also in K). The desorption order reflects the nature of the desorption process and is expressed in integer values although also non-integer values are allowed.

Ideally, the pre-exponential factor and the desorption energy are determined independently. However, since both parameters have a similar effect on the fitting routine a unique parameter set could not be found. Therefore, the pre-exponential factor is approximated by the harmonic oscillator of a solid in terms of a vibrational frequency (s^{-1}) by

$$\nu = \sqrt{\frac{2 N_s E_d(X)}{\pi^2 M}} \quad (2)$$

with $N_s \approx 10^{15} \text{ cm}^{-2}$ and M the mass of species X (Hasegawa et al. 1992). This equation gives values around 10^{12} s^{-1} . In previous papers (see e.g., Bisschop et al. 2006, Collings et al. 2003) the pre-exponential factor has been taken as a free parameter. In the present work this parameter has been linked to $E_d(X)$ following Eq.(2). For a 0th-order desorption process, ν has been multiplied with the surface density N_s , i.e. $\nu_0 = \nu \cdot N_s = \nu \cdot N_s(t=0)$. For a 1st-order process the vibrational frequency is taken as a pre-exponential factor, i.e. $\nu_1 = \nu$. Thus the only parameter that is floating in the present model fit to the experimental data is the binding energy $E_d(X)$ of the species.

Starting from Eq. (1), the kinetics are represented in terms of two coupled differential equations

$$\frac{dN_s(X)}{dt} = - \sum_{i=0,1} \nu_i [N_s(X)]^i \exp\left[-\frac{E_{d,i}(X)}{T}\right] \quad (3)$$

Table 2. Best fitting model parameters (recommended values) for CO and O₂.

| Type of ice | Reaction | Rate equation | ν [molecules ¹⁻ⁱ cm ²⁽ⁱ⁻¹⁾ s ⁻¹] | E_d [K] | i |
|--|--|---|--|--------------|-----|
| ¹² CO- ¹⁶ O ₂ | | | | | |
| Pure | CO(s) → CO(g) | $\nu_0 \exp(-E_d/T)$ | 7.2E26 | 858±15 | 0 |
| Pure | O ₂ (s) → O ₂ (g) | $\nu_0 \exp(-E_d/T)$ | 6.9E26 | 912±15 | 0 |
| Layered | CO(s) → CO(g) | $\nu_0 \exp(-E_d/T)$ | 7.2E26 | 856±15 | 0 |
| Layered | O ₂ (s) → O ₂ (g) | $\nu_0 \exp(-E_d/T)$ | 6.9E26 | 904±15 | 0 |
| Mixed | CO(s) → CO(g) | $\nu_1 [\text{CO}] \exp(-E_d/T)$ | 7.6E11 | 955±18 | 1 |
| | CO(s) → CO(g) | $\nu_0 \exp(-E_d/T)$ | 7.2E26 | 865±18 | 0 |
| Mixed | O ₂ (s) → O ₂ (g) | $\nu_0 \exp(-E_d/T)$ | 6.8E26 | 896±18 | 0 |
| ¹³ CO- ¹⁸ O ₂ | | | | | |
| Pure | CO(s) → CO(g) | $\nu_0 \exp(-E_d/T)$ | 7.0E26 | 854±10 | 0 |
| Pure | O ₂ (s) → O ₂ (g) | $\nu_0 \exp(-E_d/T)$ | 6.6E26 | 925±10 | 0 |
| Layered | CO(s) → CO(g) | $\nu_0 \exp(-E_d/T)$ | 7.1E26 | 860±15* | 0 |
| Layered | O ₂ (s) → O ₂ (g) | $\nu_0 \exp(-E_d/T)$ | 6.5E26 | 915±10 | 0 |
| Mixed | CO(s) → CO(g) | $\nu_1 [\text{CO}] \exp(-E_d/T)$ | 7.5E11 | 965±10 | 1 |
| | CO(s) → CO(g) | $\nu_0 \exp(-E_d/T)$ | 7.2E26 | 890±10 | 0 |
| Mixed | O ₂ (s) → O ₂ (g) | $\nu_0 \exp(-E_d/T)$ | 6.2E26 | 915±10 | 0 |
| Pump | | | | | |
| | CO(g) → CO(pump) | $k_{\text{pump}}[\text{CO}(\text{g})]$ | 0.00024 | - | 1 |
| | O ₂ (g) → O ₂ (pump) | $k_{\text{pump}}[\text{O}_2(\text{g})]$ | 0.00036 | - | 1 |

* Average value for ice thicknesses greater than 30 L. For ices between 20 and 30 L use 888±15 K.

$$\frac{dN_g(X)}{dt} = \sum_{i=0,1} \nu_i [N_s(X)]^i \exp\left[-\frac{E_{d,i}(X)}{T}\right] - C_x(T)k_{\text{pump}}N_g(X) \quad (4)$$

representing the density change of the solid phase (s) and gas phase (g) molecules. The last term of Eq. (4) gives the removal of gaseous species from the vacuum chamber by the pump. Here, k_{pump} is the pumping constant in s⁻¹ and $C_x(T)$ is a dimensionless cryo-pumping factor between 1 and 7 as discussed in §2. The pumping constant, k_{pump} , is constrained by fitting the pump down curve of both species, i.e., the slope of the TPD curve at temperatures higher than the desorption peak temperature. In most cases, the peak tail is not well reproduced due to the presence of other cold surfaces in the system. Very small amounts of gas that have missed the target can get deposited and can be desorbed afterwards at a temperature different from that of the target surface. A direct consequence is a deviation in model curves from the experimental plots at high temperatures. However, this does not affect the determination of the binding energies that are mainly sensitive to the peak value and the leading edge.

In order to calculate the temperature dependent rate measured in the TPD experiments, dn/dt is written as

$$\frac{dn}{dt} = \frac{dn}{dT} \frac{dT}{dt} = \beta \frac{dn}{dT} \quad (5)$$

with dn/dT the temperature dependent rate (molecules cm⁻²K⁻¹), and $\beta = dT/dt$ the constant TPD heating rate (K s⁻¹) that corresponds to 0.1 K/minute in the present study unless stated differently.

To extract the binding energy from the observations a standard minimization of χ^2 is used which represents the sum

over the squares of the differences between the experimental points and the calculated ones. In this procedure first a 0th- or 1st-order process is fitted and subsequently the appropriate parameters are optimized.

4.2. Results

The results are shown in Figs. 4 and 5 and Table 2 summarizes the model equations with best fit parameters. In nearly all experiments a linear dependence between ice thicknesses and desorption energies has been found.

Pure ices. For pure ¹⁸O₂ five experiments are performed using different thicknesses (20 L, 40 L, 50 L, 60 L, 80 L) and the best fits to these experiments (Fig. 4b) give 932, 927, 924, 928 and 918 K, respectively, corresponding to an average value of 925 ± 10 K. The error of the mean value is chosen to give a conservative estimate of these parameters. Similarly, for pure CO (Fig. 4a) the binding energy is 854 ± 10 K which is consistent with the value of 855 K reported by Öberg et al. (2005) and Bisschop et al. (2006). Both pure CO and pure O₂ ice exhibit 0th-order kinetics. The TPD spectra are reproduced very well with this model using only one free parameter as is demonstrated in Figs. 4a and b, where the experimental and model results are plotted on top of each other. In Fig. 4d the variations of χ^2 for the experiments of 40 L for the pure CO and O₂ are shown. The energy values for which χ^2 is minimum are taken as the final values. This yields 854 K for ¹³CO and 927 K for ¹⁸O₂. As mentioned in the experimental section we have explicitly taken into account the effect of cryo-pumping. A systematic deviation of 2 to 3 K in the desorption energy is induced when this factor is neglected. This is illustrated in Fig. 4d. Inclusion of the $C_x(T)$ function generally improves the fit substantially.

¹²CO and ¹⁶O₂ show a similar desorption behavior and the binding energies are 858 ± 15 K and 912 ± 15 K, respec-

tively. Thus ¹²CO has the same binding energy as ¹³CO within the errors. For ¹⁶O₂ ices the binding energy is lowered by 1.6% with respect to ¹⁸O₂ on average. Because of the smaller data set for the main isotope the errors in the fitted parameters of the ¹²CO and ¹⁶O₂ isotopes are larger than those for ¹³CO and ¹⁸O₂.

Layered ices. The desorption of ¹⁸O₂ in 1/1 (Fig. 5d) and x/40 (Fig. 5c) layered ices is 0th-order and the binding energy is determined as 915 ± 10 K, which is slightly lower than for the pure ices. ¹⁶O₂ shows a similar behavior with a binding energy of 904 ± 10 K. ¹³CO desorption is a 0th-order process and only at low coverages a 1st-order process may be involved. Since there is no signature in the TPD spectra (nor in the RAIR spectra) of mixing or segregation and since the spectrum looks very similar to pure ices it is modeled in 0th-order with an average binding energy of 860 ± 15 K for ices thicker than 30 L. The correctness of this procedure is confirmed by the TPD spectra of ¹²CO which exhibit a 0th-order desorption with a binding energy of 856 ± 15 K.

Mixed ices. O₂ in mixed ices (Fig. 5c) is again 0th-order with a similar binding energy as in layered ices. In mixed ices, TPD spectra of ¹³CO are broader with respect to pure ices and a shoulder around the desorption temperature of O₂ is observed. This suggests that CO is desorbing from a wider range of binding sites and this is also supported by RAIR spectra that are broader with respect to pure ice spectra. Both the peak and shoulder are fitted very well using a combination of 0th- and 1st-order processes (see Fig. 5a). About 50% of the CO desorbs from CO-CO binding sites as in the pure ices but with a binding energy of 890 ± 10 K. The residual CO molecules desorb through a 1st-order process from a mixed environment, i.e. including CO-O₂ binding sites, with a binding energy of 965 ± 5 K.

Table 2 has separate entries for the ¹³CO-¹⁸O₂ and ¹²CO-¹⁶O₂ isotopomers. Independent of the used isotopomers it can be concluded that the binding energies of CO increase in the following order $E_{\text{pure}} \lesssim E_{\text{layered}} < E_{\text{mixed}}$. For O₂ this is inverted $E_{\text{pure}} > E_{\text{layered}} \gtrsim E_{\text{mixed}}$.

The effect of β on the binding energies. In order to rule out any dependencies on the adopted heating rates, experiments have been performed for $\beta=0.1, 0.2$ and 0.5 K min⁻¹ on 40 L CO ices. This is of relevance when applying laboratory values to interstellar warm-up time scales. The calculated ν and E_d values for the 0.5 K min⁻¹ experiment have been used to predict the experimental TPD curve for 0.2 and 0.1 K min⁻¹. The deviation between the calculated and experimental values are within the experimental error, i.e. $\Delta E_d = \pm 15$ K, with a slight tendency for lower inferred E_d at lower heating rates.

4.3. Sticking probability

In addition to the desorption rates, the sticking coefficients also play an important role to describe freeze-out onto interstellar grains. The measurement procedure has been extensively discussed in Bisschop et al. (2006) and Fuchs et al. (2006). It is important to note that the measurements only provide an ‘uptake’ coefficient γ rather than a sticking coefficient, S , as only the net rate of molecules sticking and leaving the surface can be given. Consequently, the values given in Fig. 6 represent lower limits for the sticking

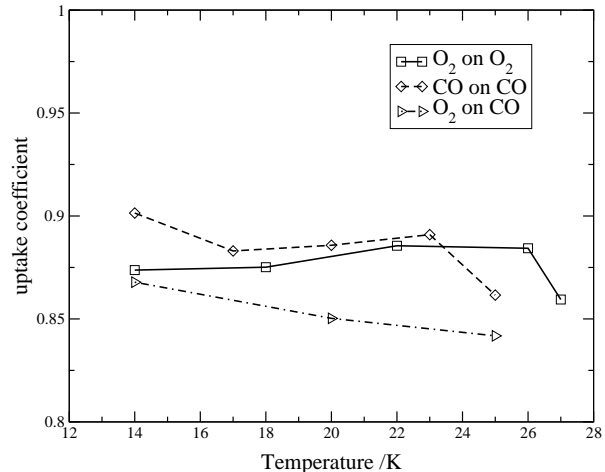


Fig. 6. Uptake coefficient γ representing the lower limits on the sticking coefficients as functions of the temperature below 25 K.

coefficients of O₂ and CO. It is found that the freeze-out dominates for O₂ on O₂, CO on CO and O₂ on CO up to 25 K with lower limits on the sticking probabilities between 0.85 and 0.9, i.e., close to unity. Under real astrophysical conditions this value will increase and approaches unity at 10 K.

5. Astrophysical implications

The scenarios put forward to explain the absence of gaseous O₂ in interstellar clouds can roughly be divided into two categories: time-dependent models of cold cores invoking freeze-out of oxygen (in all its forms) onto grains (e.g., Bergin et al. 2000, Aikawa et al. 2005), and depth-dependent models of large-scale warm clouds invoking deep penetration by UV radiation in a clumpy structure enhancing the O₂ photodissociation (e.g., Spaans & van Dishoeck 2002). The laboratory experiments presented here are relevant to the first scenario. In these models, atomic O is gradually transformed with time into O₂ in the gas phase. Freeze-out of oxygen occurs on a similar timescale, and any O is assumed to be turned effectively into H₂O ice on the grains where it subsequently sticks. No formation of solid O₂ on the grain is expected because of the presence of atomic hydrogen, which is much more mobile at low temperatures. The H₂O ice formation lowers the gaseous [O]/[C] ratio and potentially leaves only a small abundance of O₂ in the gas. The amount of solid O₂ and the remaining fraction of gaseous O₂ of $\sim 10^{-8} - 10^{-7}$ with respect to H₂ depends sensitively on the temperature at which O₂ is frozen out. A related question is to what extent O₂ differs in this respect from CO, since CO is readily observed in the gas phase and in solid form.

Astrochemical models usually assume 1st-order desorption with rates in cm⁻³ s⁻¹. Appendix A (see online material) summarizes the equations used to apply our laboratory results to astrochemical models for both 1st and 0th order kinetics. The latter is more appropriate for thick ices in interstellar clouds and consistent with our laboratory data. We consider the simple case of pure desorption and accretion of ¹²CO and ¹⁶O₂, without any gas-phase or solid-state

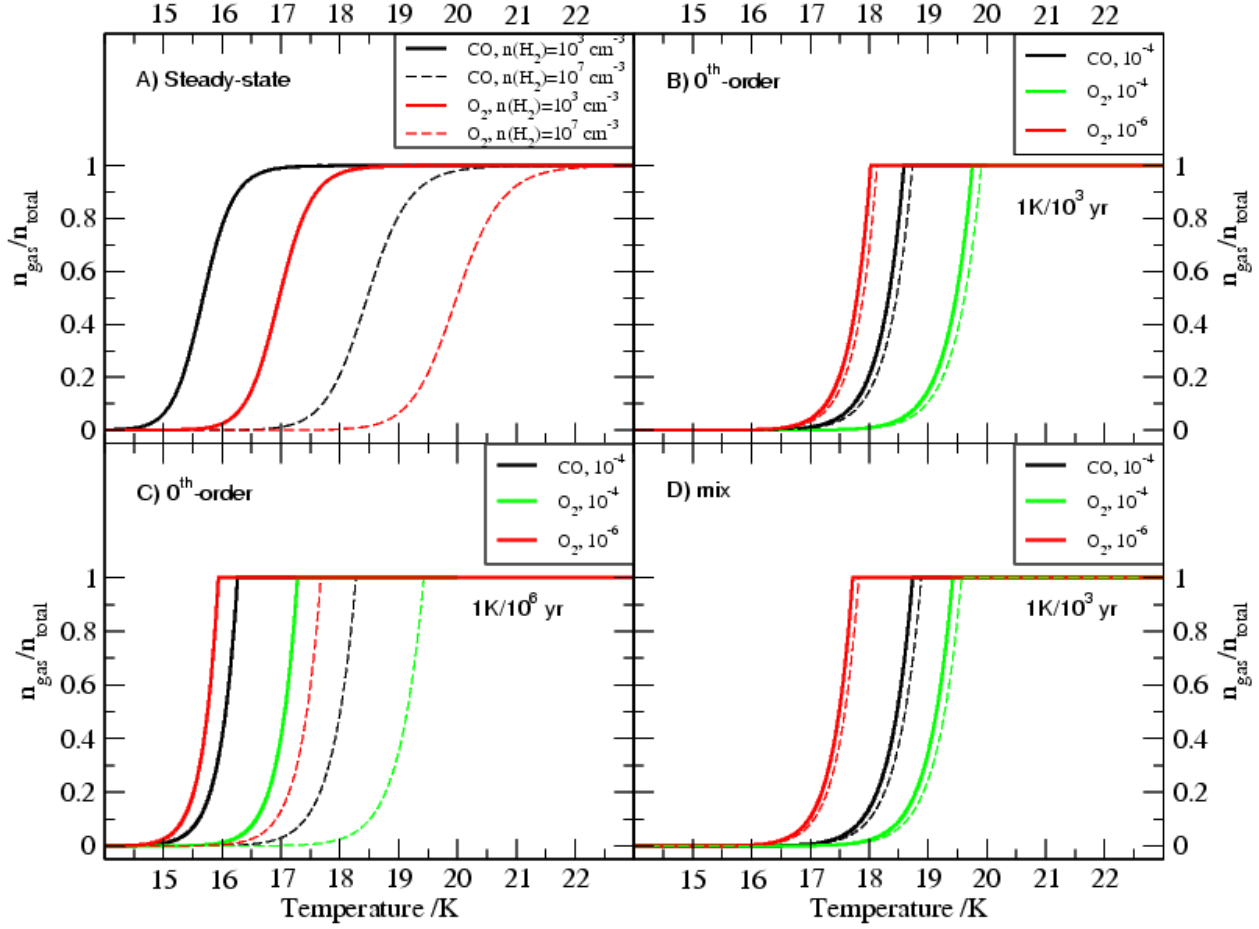


Fig. 7. Astrophysical simulations of gaseous CO and O₂ abundances relative to the total gas + solid abundances. Panel (a) shows pure CO and O₂ in steady-state, panel (b) 0th-order desorption for heating rates of 1 K/1000 yr, panel (c) the same but for 1 K/10⁶ yr, and panel (d) shows the desorption of CO from mixed (layered) ices for 1 K/10³ yr. In the panels (b)-(d) the solid line indicates accretion corresponding to $n(\text{H}_2)=10^3 \text{ cm}^{-3}$, the dashed line corresponds to accretion for $n(\text{H}_2)=10^7 \text{ cm}^{-3}$. For the panels (b)-(d) the adopted initial gaseous abundances of CO is 10^{-4} and for O₂ it is 10^{-4} and 10^{-6} with respect to H₂.

chemistry. Thus, the main difference with the equations in §4.1 is that desorption is now balanced by a freeze-out (accretion) term, rather than a pumping factor. Also, the laboratory heating rate can be replaced by a heating rate appropriate for the astrophysical object under consideration, for example a protostar heating its envelope.

Our model only considers classical dust grains with a radius of 0.1 μm . The density $n(\text{H}_2)$ is varied to simulate the effects for clouds of different densities. In 0th order, the results depend on the initial number densities of the CO and O₂ molecules. For CO, an abundance 10^{-4} relative to H₂ is chosen, initially all on the grains. For O₂, two options are considered. The first option is that most oxygen has been converted into O₂ at an abundance of 10^{-4} , as found in gas-phase models and the maximum allowed by the observed upper limits on solid O₂. The second case considers a much lower O₂ abundance of 10^{-6} , as found in gas-grain models.

Fig. 7a shows the results for pure CO and pure O₂ ices in the simplest case of steady-state. The temperature at which these species desorb depends strongly on density: the higher the density, the faster the accretion rate which needs to be balanced by desorption. Because of the larger

binding energy of O₂, it always desorbs at ~ 2 K higher temperatures than CO.

Fig. 7b shows the result for 0th order desorption at a heating rate typical for a proto-stellar environment of 1 K/1000 yr (Lee et al. 2005). For abundances of CO and O₂ of 10^{-4} , both species desorb at ~ 2.5 K higher temperatures than the steady-state case at low densities; at high densities, there is little difference. If the O₂ abundance is lowered to 10^{-6} the 0th order curve shifts to lower temperature by ~ 2 K. Thus, in contrast with the steady-state or equal abundance cases, O₂ can desorb at *lower* temperatures than CO if its abundance is significantly lower. This reversal is a specific feature of the 0th order desorption and is not found in the 1st order formulation (see Appendix A in the online version). An important question is whether such a situation is astrochemically relevant. For O₂ abundances as low as 10^{-6} , the coverage becomes less than a mono-layer and 1st order kinetics or other effects due to the peculiarities of the ice (e.g. polar vs. apolar environment, compact vs. porous ice) will determine the desorption behavior.

Fig. 7c shows the abundance curve of the species for a heating rate of 1 K/10⁶ yr, as expected for a cold core

at near constant temperature. Since the time scale is increased by 3 orders of magnitude with respect to the previously considered heating rate there is simply more time for the molecules to desorb and consequently the entire profile shifts to lower temperatures by 0.5 – 2.5 K depending on the density of the species.

Finally, Fig. 7d shows the abundance curves of CO and O₂ from mixed ices. The graphs of mixed and layered ices are nearly identical, thus the layered ices are not shown separately. The relative abundance curve is shifted to a higher temperature by about 0.5 K compared with the pure ices because of the slightly higher binding energies.

Overall, Fig. 7 shows that the differences in the desorption behavior of O₂ and CO with temperature are very minor for a wide range of realistic cloud densities and abundances. Thus, it is unlikely that a large reservoir of solid O₂ is hidden in the bulk of molecular clouds which show abundant gaseous CO but no O₂, unless the O₂ is in a more strongly bound ice environment. Conversely, any region with significant CO freeze-out should also have some solid O₂. As noted in the introduction, the best limits come from analysis of the weak solid ¹³CO band, which gives upper limits of 100% on the amount of O₂ that can be mixed with CO, i.e., about $(0.5 - 1) \times 10^{-4}$ with respect to H₂ (Boogert et al. 2003, Pontoppidan et al. 2003). Direct freeze-out of the gas-phase O₂ abundances inferred from the ODIN measurements would give much lower limits.

The small differences between CO and O₂ desorption found here may become relevant in the interpretation of high spatial resolution observations of individual cold cores with temperatures in the 10–20 K range such as the pre-stellar core B68.

6. Concluding remarks

The desorption processes of CO-O₂ pure, mixed and layered ice systems have been investigated experimentally and modeled using an empirical kinetic model. The resulting molecular parameters can be used to model the desorption behavior of these ices under astrophysical conditions. We find that both pure ¹⁶O₂ and pure ¹²CO desorb through 0th-order processes with binding energies of 912 ± 15 K and 858 ± 15 K, respectively. In mixed and layered ices the ¹⁶O₂ binding energy decreases to a lower value around 896 ± 18 K and 904 ± 15 K respectively. The ¹²CO desorption from layered ices is 0th-order with a binding energy of 856 ± 15 K. In mixed ices a combination of 0th- and 1st-order is found with desorption energies of 865 ± 18 K and 955 ± 18 K, respectively. For ¹⁸O₂ and ¹³CO, these numbers change by a few percent.

O₂ is less volatile than CO but CO does not co-desorb with O₂. This is in contrast with the CO-N₂ ice system for which Bisschop et al. (2006) found that N₂ is more volatile than CO and that significant amounts of N₂ co-desorb with CO. The sticking coefficients of CO and O₂ at temperatures below 20 K are close to unity, with 0.85 as a lower limit. In cold clouds ($T_d < 18$ K), O₂ can be frozen out onto the grains, but the relative difference in desorption between CO and O₂ is so small that this is unlikely to be the explanation for the missing gaseous O₂ in interstellar clouds which show significant gaseous CO.

in the construction of the experimental setup. We acknowledge funding through the Netherlands Research School for Astronomy (NOVA), FOM and a Spinoza Grant from the Netherlands Organization for Scientific Research (NWO). K.A. thanks the Greenberg family for a Greenberg research fellowship and the ICSC-World Laboratory Fund for additional funding.

References

- Bergin, E. A., Langer, W. D., & Goldsmith, P. F. 1995, ApJ, 441, 222
 Bergin, E. A., Melnick, G. J., Stauffer, J. R., et al. 2000, ApJ, 539, L129
 Bisschop, S. E., Fraser, H. J., Öberg, K. I., van Dishoeck, E. F., Schlemmer, S., 2006, A&A, 449, 1297
 van Broekhuizen, F. A. 2005, PhD thesis, Leiden University
 Chiar, J. E., Gerakines, P. A., Whittet, D. C. B., Pendleton, Y. J., Tielens, A. G. G. M., Adamson, A. J., & Boogert, A. C. A. 1998, ApJ, 498, 716
 Collings, M., Dever, J., Fraser, H., & McCoustra, M. 2003, ApJS, 285, 633
 Collings, M. P., Anderson, M. A., Chen, R., Dever, J. W., Viti, S., Williams, D. A., & McCoustra, M. R. S. 2004, MNRAS, 354, 1133
 Dartois, E., 2006, A&A, 445, 959
 D’Hendecourt, L. B., Allamandola, L. J., & Greenberg, J. M. 1985, A&A, 152, 130
 Ehrenfreund, P., Breukers, R., d’Hendecourt, L., Greenberg, J.M., 1992, A&A, 260, 431
 Ehrenfreund, P., Boogert, A., Gerakines, P., Tielens, A., & van Dishoeck, E. 1997, A&A, 328, 649
 Ehrenfreund P. & van Dishoeck E. 1998, Adv. Space. Res., 21, 15
 Elsila, J., Allamandola, L. J., & Sandford, S. A. 1997, ApJ, 479, 818
 Fraser, H. J., Collings, M. P., McCoustra, M. R. S. and Williams, D. A. 2001, MNRAS, 327, 1165
 Fuchs, G.W., Acharyya, K., Bisschop, S.E., et al., 2006, Far. Disc., 133, 331
 Goldsmith, P. F., Melnick, G. J., Bergin, E. A., et al. 2000, ApJ, 539, L123
 Hasegawa, T. I., Herbst, E., & Leung, C. M. 1992, ApJS, 82, 167
 Léger, A., 1983, A&A, 123, 271
 Liseau, R. & Odin Team. 2005, in Astrochemistry: recent successes and current challenges, IAU Symposium No 231, eds. Lis, D., Blake, G.A., Herbst, E. (Cambridge University Press), p. 301
 Meyer, D.M., Jura, M, Cardelli, J.A., 1998, ApJ, 493, 222
 Öberg, K. I., van Broekhuizen, F., Fraser, H. J., van Dishoeck, E. F., Schlemmer, S., 2005, ApJ, 621, L33
 Pagani, L., Olofsson, A. O. H., Bergman, P., 2003, A&A, 402, L77
 Pontoppidan, K. M., Fraser, H. J., Dartois, E., et al. 2003, A&A, 408, 981
 Vandenbussche, B., Ehrenfreund, P., Boogert, A. C. A., et al. 1999, A&A, 346, L57

Online Material

Appendix A: Modeling accretion and desorption in astrochemical applications

The gas-phase density $n_g(X)$ (in cm⁻³) of species X with respect to its total gas + solid density $n_{\text{tot}}(X) = n_g(X) + n_s(X)$ can be calculated from the accretion and desorption rates. For reasons of simplicity and to compare with other work we consider here the simplest case of a single type of grain with a classical radius $r_c=0.1 \mu\text{m}$, 10^{15} sites per cm² and a grain abundance $n_{gr}/n(\text{H}_2)=10^{-12}$.

A.1. Accretion rate

The most general formulation of the accretion rate in cm⁻³ s⁻¹ is

$$R_{\text{acc}} = \sigma S v n_g(X) n_{gr} \quad (\text{A.1})$$

where $\sigma=\pi r_c^2$ is the grain cross section, S is the sticking coefficient (taken to be unity at $T_{gr} < 20$ K) and v is the mean speed of the gas in cm s⁻¹. For a classical grain and the canonical grain abundance this becomes

$$R_{\text{acc}} = 4.55 \times 10^{-18} \left(\frac{T}{M(X)} \right)^{0.5} n_g(X) n_{\text{H}_2} \quad (\text{A.2})$$

where T is the gas temperature and $M(X)$ is the mass of X in atomic mass units (amu). The accretion rate per molecule X in s⁻¹ is denoted as

$$\lambda = R_{\text{acc}}/n_g(X) \quad (\text{A.3})$$

and the timescale for freeze-out can be computed from $\tau = 1/\lambda$. Note that in dense cold cores, the grains may have grown to larger μm sizes than assumed here due to coagulation, in which case the abundance has to be lowered. Also, a more sophisticated calculation should include a grain size distribution.

A.2. Desorption rate

The desorption rate in the laboratory surface science experiments is given by Eq. (1) in cm⁻² s⁻¹, which is rewritten here as

$$R_{\text{des,lab}} = \nu_i N^i \exp\left[-\frac{E_i}{kT_{gr}}\right] \quad (\text{A.4})$$

where N has the units of molecules cm⁻², and the unit of ν_i changes with the order i of desorption as molecules¹⁻ⁱ cm²⁽ⁱ⁻¹⁾ s⁻¹. For 0th-order ν_0 is in molecules cm⁻² s⁻¹ and for 1st-order ν_1 is in s⁻¹. E_i is the binding energy for order i .

A.2.1. 1st order

For 1st order kinetics, the translation from the laboratory data to a astronomical desorption rate ξ in s⁻¹ is straightforward:

$$\xi_1 = \nu_1 \exp\left[-\frac{E_1}{kT_{gr}}\right] \quad (\text{A.5})$$

with ν_1 and E_1 taken directly from the laboratory data. The rate R_{des} in cm⁻³ s⁻¹ becomes

$$R_{\text{des}} = \xi_1 n_s(X) = \nu_1 n_s(X) \exp\left[-\frac{E_1}{kT_{gr}}\right] \quad (\text{A.6})$$

with n_s (in cm⁻³) the density of molecules on the grain surface.

A.2.2. 0th order

For 0th order kinetics, the desorption rate R_{des} in cm⁻³ s⁻¹ should be proportional to the number density of grains n_{gr} and the average surface area A_{gr} of a grain. The rate ‘per grain’ in s⁻¹ can be obtained from

$$\xi_0 = \nu_0 A_{gr} \exp(-E_0/kT_{gr}) \quad (\text{A.7})$$

with ν_0 and E_0 derived from the laboratory data for 0th order. The total rate is

$$R_{\text{des}} = \xi_0 n_{gr} = \nu_0 A_{gr} n_{gr} \exp(-E_0/kT_{gr}) \quad (\text{A.8})$$

A.3. Steady-state model

If no chemical reactions in the gas or on the grains are included, a steady-state will be reached where the accretion balances the desorption. In 1st order, this becomes

$$\lambda n_g(X) = \xi_1 n_s(X) \quad (\text{A.9})$$

with ξ_1 from Eq. A.5. Thus the ratio of gas-phase to solid-state molecules is given by

$$\frac{n_g}{n_s} = \frac{\xi_1}{\lambda} = 2.2 \cdot 10^{17} \nu_1 \sqrt{M} \frac{\exp(-E_1/kT_{gr})}{\sqrt{T}} \quad (\text{A.10})$$

Results of Eq.A.10 are shown in Fig. A.1 for two densities $n(\text{H}_2)=10^3$ and 10^7 cm⁻³. No heating rate β is involved in this calculation. It is the most simple ‘astrochemical’ modeling result achievable. One note of caution, however: it is not correct to use laboratory values for E_i which were fitted to 0th-order laboratory data for 1st-order astrochemical equations and just change ν . If 1st order kinetics are used (even though the laboratory data indicate 0th order), a better approach would be to first fit the laboratory data with 1st order kinetics and then apply those in the astrochemical models. The differences in binding energies can be as large as 12% for CO and O₂. For pure N₂, CO and O₂, 1st order fits to the peaks of our laboratory curves give 800 K, 955 K and 1035 K, respectively, with $\nu_1 = 1.0 \cdot 10^{11}$ s⁻¹ for N₂ (Bisschop et al. 2006) and $\nu_1 = 1.0 \cdot 10^{12}$ s⁻¹ for CO and O₂. Figures 7a and A.1 use these values.

A.4. Time-dependent model

A.4.1. 1st order

In the 1st order approach, the desorption rate changes with the number of species X bound to the grain, which is justified only for (sub)monolayer or irregular coverage. In this scenario the abundance of a species is determined by two differential equations and some boundary (initial) conditions

$$\begin{aligned} dn_g/dt &= -\lambda n_g + \xi_1 n_s \\ dn_s/dt &= +\lambda n_g - \xi_1 n_s. \end{aligned} \quad (\text{A.11})$$

These are the equations commonly used in time-dependent astrochemical models (e.g., Bergin & Langer 1997, Charnley et al. 2001, Aikawa et al. 2005).

For protostellar cores in which a star turns on, the simplest assumption is that there is a linear relation between the temperature T_{gr} and the time t

$$T_{gr}(t) = T_{gr,0} + dT_{gr}/dt \cdot t = T_{gr,0} + \beta t \quad (\text{A.12})$$

with $T_{gr,0}$ around 10 K. At $t = 0$, all molecules are assumed to be frozen out onto grains, $n_s(t = 0) = n_{tot}(X)$, as appropriate for a pre-stellar core prior to star formation. A completely opposite situation, not studied here, would be a quiescent cloud where dT_{gr}/dt is close to zero and a molecules are initially in the gas phase. Note that in this case the timescales are dominated by the freeze-out process rather than the evaporation timescale, and that this result in a very different time behavior, depending on temperature.

Fig. A.1 includes the time-dependent 1st order result for a heating rate of 1 K per 10^3 yr and two densities. Compared with the steady-state results, the low density curves are shifted to higher temperatures by ~ 3 K, whereas the high density curves are nearly identical. A slower heating rate of 1 K per 10^6 yr brings the low density curve closer to the low density steady-state results.

A.4.2. 0th order

In the 0th order approach, the desorption rate is constant with time, independent of the surface density $n_s(X)$. The time-dependent equations now become

$$\begin{aligned} \frac{dn_g}{dt} &= -\lambda n_g + R_{des} & \text{for } n_s > 0 \\ &= -\lambda n_g & \text{for } n_s = 0 \\ \frac{dn_s}{dt} &= +\lambda n_g - R_{des} & \text{for } n_s > 0 \\ &= +\lambda n_g & \text{for } n_s = 0 \end{aligned} \quad (\text{A.15})$$

with R_{des} from Eq. A.8. This formulation is most appropriate for thick, fully covered ice layers. For partial coverage R_{des} would need to be multiplied by a relative surface occupation number θ between 0 and 1, but for the cases of pure CO and O₂ ices considered here $\theta=1$ is taken. The condition on the right hand side causes an abrupt end to the desorption process once the molecules on the surface have been evaporated. Instead of getting a smooth S-shaped curve like in the 1st-order approach, the density curve of a 0th-order formulation reveals a sharp edge at the end of the evaporation process.

The results now depend on the choice of the initial $n_g(X)/n(\text{H}_2)$ abundance ratio of species X . For CO, a logical choice is $n_g(\text{CO})/n(\text{H}_2) = 10^{-4}$. For O₂, an extreme case would be to put all oxygen into O₂, $n_g(\text{O}_2)/n(\text{H}_2) > 10^{-4}$. However, models and observations (see §1) suggest that a more plausible abundance is at least two orders of magnitude lower. Figure A.1 shows the results for $n_g(\text{O}_2)/n(\text{H}_2) = 10^{-6}$ and 10^{-4} . The 0th order curves for CO and O₂ for 10^{-4} differ by less than 0.7 K from those at 1st order. However, those for O₂ at 10^{-6} are shifted to lower temperature by ~ 2.5 K.

These examples illustrate the importance of proper modeling of both the order of the desorption processes involved and the balance with accretion. Shifts of a few K compared to the steady-state solution can occur either way depending on cloud parameters. Such small shifts are unlikely to affect the interpretation of large-scale molecular clouds, but they may potentially become significant in interpretations of the relative behavior of CO, O₂ and N₂ in cold dense clouds in the 10–20 K range.

Finally, it should be noted that our results using the empirical model for pure ices are consistent with first principle

considerations using saturated vapor pressure equations, as done for pure CO by Léger (1983).

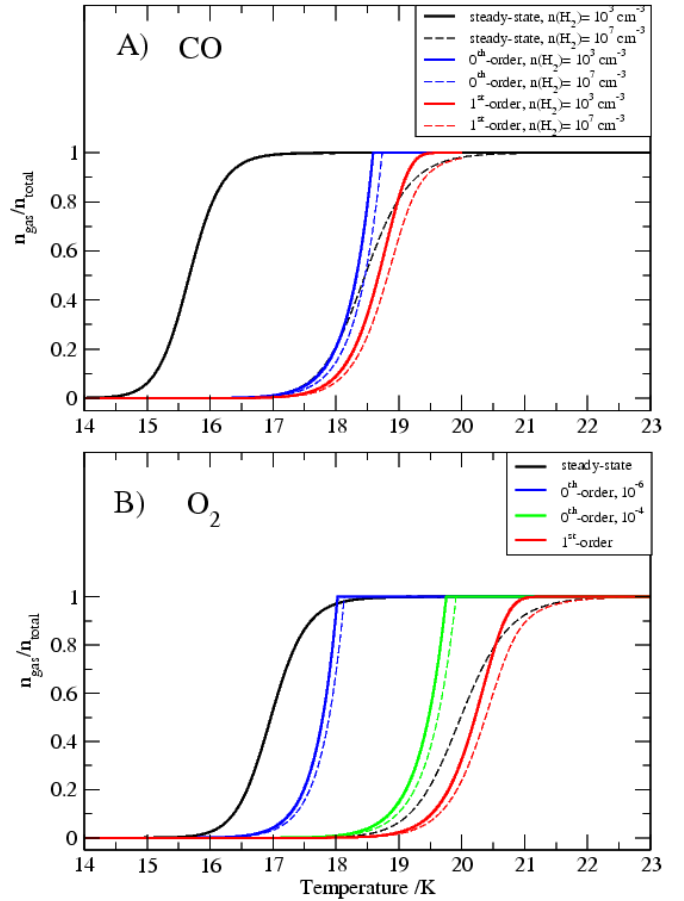


Fig. A.1. The gas-phase fraction of CO (top) and O₂ (bottom) for densities of $n(\text{H}_2)=10^3 \text{ cm}^{-3}$ (full lines) and 10^7 cm^{-3} (dashed lines) in the case of pure ices. Both steady-state (black), 0th-order (blue/green) and 1st-order (red) desorption are considered. In 0th order, the adopted abundance for CO is 10^{-4} whereas for O₂ both 10^{-4} (green) and 10^{-6} (blue) are considered.